LOYOLA UNIVERSITY CHICAGO 1870 AD MAJOREM DEI GLORIAM eCOMMONS

Loyola University Chicago
Loyola eCommons

Chemistry: Faculty Publications and Other Works

Faculty Publications and Other Works by Department

3-16-2021

Atomic-Resolution 1.3 Å Crystal Structure, Inhibition by Sulfate, and Molecular Dynamics of the Bacterial Enzyme DapE

Matthew Kochert
Loyola University Chicago

Boguslaw P. Nocek
University of Chicago

Thahani S. Habeeb Mohammad
Loyola University Chicago

Elliot Gild
Loyola University Chicago

Kaitlyn Lovato
Loyola University Chicago

See next page for additional authors

Follow this and additional works at: https://ecommons.luc.edu/chemistry_facpubs

 Part of the Chemistry Commons

Author Manuscript
This is a pre-publication author manuscript of the final, published article.

Recommended Citation

Kochert, Matthew; Nocek, Boguslaw P.; Habeeb Mohammad, Thahani S.; Gild, Elliot; Lovato, Kaitlyn; Heath, Tahirah K.; Holz, Richard C.; Olsen, Kenneth W.; and Becker, Daniel P. Ph.D.. Atomic-Resolution 1.3 Å Crystal Structure, Inhibition by Sulfate, and Molecular Dynamics of the Bacterial Enzyme DapE. Biochemistry, 60, 12: 908–917, 2021. Retrieved from Loyola eCommons, Chemistry: Faculty Publications and Other Works, http://dx.doi.org/10.1021/acs.biochem.0c00926

This Article is brought to you for free and open access by the Faculty Publications and Other Works by Department at Loyola eCommons. It has been accepted for inclusion in Chemistry: Faculty Publications and Other Works by an authorized administrator of Loyola eCommons. For more information, please contact ecommons@luc.edu.

This work is licensed under a Creative Commons Attribution-Noncommercial-No Derivative Works 3.0 License.
© American Chemical Society, 2021.

Authors

Matthew Kochert, Boguslaw P. Nocek, Thahani S. Habeeb Mohammad, Elliot Gild, Kaitlyn Lovato, Tahirah K. Heath, Richard C. Holz, Kenneth W. Olsen, and Daniel P. Becker Ph.D.

This article is available at Loyola eCommons: https://ecommons.luc.edu/chemistry_facpubs/120

Atomic-Resolution 1.3 Å Crystal Structure, Inhibition by Sulfate, and Molecular Dynamics of the Bacterial Enzyme DapE

Matthew Kochert[a§], Boguslaw P. Nocek[b], Thahani S. Habeeb Mohammad[a], Elliot Gild[a], Kaitlyn Lovato[a], Tahirah K. Heath[a], Richard C. Holz[c], Kenneth W. Olsen[a]*, and Daniel P. Becker[a]*

[a]Department of Chemistry and Biochemistry, Loyola University Chicago, 1032 West Sheridan Road, Chicago, IL 60660; [b]The Center for Structural Genomics of Infectious Diseases, Computation Institute, University of Chicago, Chicago, Illinois, 60637; [c]Department of Chemistry, Colorado School of Mines, 1500 Illinois St., Golden, CO 80401, U.S.A.

KEYWORDS: diaminopimelate desuccinylase, DapE, targeted molecular dynamics, enzyme mechanism, inhibition by sulfate, protein hinge flexibility

Abstract

We report the atomic resolution (1.3 Å) X-ray crystal structure of the open conformation of the *dapE*-encoded *N*-succinyl-L,L-diaminopimelic acid desuccinylase (DapE, E.C. 3.5.1.18) from *Neisseria meningitdis*. This structure (PDB 5UEJ) contains two bound sulfate ions in the active site that mimic the binding of the terminal carboxylates of the *N*-succinyl-L,L-diaminopimelic acid (L,L-SDAP) substrate. We demonstrated inhibition of DapE by sulfate (IC_{50} = 13.8 ± 2.8 mM). Comparison with other DapE structures in the PDB demonstrates the flexibility of the inter-domain connections of this protein. This high-resolution structure was then utilized as the starting point for targeted molecular dynamics experiments revealing the

conformational change from the open form to the closed form that occurs when DapE binds L,L-SDAP and cleaves the amide bond. These simulations demonstrated closure from the open to the closed conformation, the change in RMS throughout the closure, and the independence in the movement of the two DapE subunits. Although there was no targeting force, the substrate moved closer to the active site and bound more tightly during the closure event.

Introduction

The rapid rise in morbidity and mortality from bacterial infections caused by antibiotic-resistant bacteria[1] underlines the need to discover antibiotics with a new mechanism of action by targeting previously unexplored bacterial enzymes. For example, invasive methicillin-resistant *Staphylococcus aureus* (MRSA) is a serious and growing health problem.[2] Several newly discovered strains of MRSA show antibiotic resistance even to vancomycin, which is considered a last resort for the treatment of systemic infections.[3] An attractive but underexplored bacterial target that is present in all Gram-negative and most Gram-positive bacteria is the *dapE*-encoded *N*-succinyl-L,L-diaminopimelic acid desuccinylase (DapE, E.C. 3.5.1.18).[4] DapE is a member of the lysine biosynthetic pathway in bacteria that is responsible for the synthesis of lysine and *meso*-diaminopimelate (*m*-DAP),[5] both of which are critical for peptidoglycan cell-wall synthesis. DapE enzymes catalyze the hydrolysis of *N*-succinyl-L,L-diaminopimelic acid (L,L-SDAP) to succinate and L,L-diaminopimelic acid (L,L-DAP, Figure 1).

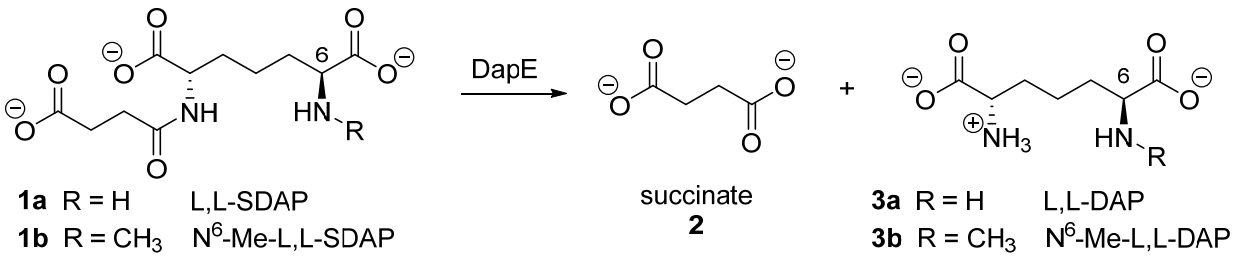

Figure 1. Hydrolysis of L,L-SDAP by DapE. L,L-SDAP (**1a**) and assay substrate N^6-methyl-L,L-SDAP[6] (**1b**) with formation of hydrolysis products succinate (**2**) and L,L-diaminopimelic acid derivatives **3a** and **3b**, respectively.

Deletion of the *dapE* gene is lethal to *Helicobacter pylori* and *Mycobacterium smegmatis*, demonstrating the indispensable role of this enzyme in bacterial survival, and therefore pathogenesis in the human host.[7, 8] Furthermore, lack of a similar pathway in humans suggests that inhibition of DapE should be selectively toxic to bacteria but not human hosts, making it a promising target for antibiotics with a new mechanism of action free of mechanism-based side effects.[4] To conveniently measure the inhibitory potency of test compounds versus DapE, we previously reported a ninhydrin-based assay[6] employing the substrate N^6-methyl-L,L-SDAP (**1b**), which when cleaved by DapE affords the primary amine product **3b** (Fig. 1) that can be quantified spectrophotometrically after treatment with ninhydrin.

The first X-ray crystal structure of an apo DapE from *Neisseria meningitidis* (*Nm*DapE) was solved in 2005,[9] and was followed by structures of mono- and di-Zn forms from *Haemophilus influenzae* (*Hi*DapE)[10] and mono- and di-Zn forms from *Nm*DapE.[11] Significantly, the structure of the DapE inhibitor captopril bound to the active site demonstrated interactions of the thiol moiety with the active site zinc atoms.[11] We recently reported a DapE crystal structure revealing the previously-unknown closed conformation of dimeric DapE with the products of enzymatic cleavage, succinate and diaminopimelic acid, bound in the active site (PDB 5VO3).[12] This structure also revealed the role of His195B, a residue on the opposite subunit that moves ~10 Å and provides a key H-bond to the substrate in the active site.[12] The requirement of this

His residue explains the observed inactivity of a truncated, monomeric construct of DapE.[6] The products bound structure, aided by our products-bound transition state modeling (PBTSM) approach,[12, 13] enabled further refinement of the proposed reaction mechanism of DapE that will facilitate inhibitor identification[14-16] for the discovery of new antibiotics that inhibit DapE.

We report herein a new atomic-resolution (1.3 Å) X-ray crystal structure of *Nm*DapE (PDB 5UEJ) with sulfate ions bound in the substrate recognition pocket. Our previous closed products-bound structure of *Hi*DapE[12] in combination with this new high-resolution open structure further defines the dramatic conformational range of motion that occurs for DapE during its catalytic cycle and enabled us to explore this remarkable conformational process using targeted molecular dynamics (TMD).

Experimental

Protein Preparation and Crystallization

*Nm*DapE was expressed in *E. coli* and prepared according to a protocol described previously.[6, 11, 12] Bacteria were cultured with shaking at 210 rpm in LB medium supplemented with 150 μg/ml ampicillin at 37°C until the OD_{600} reached 1.0. The temperature was lowered to 18°C and isopropyl-D-thiogalactopyranoside (IPTG) was added to a final concentration of 0.5 mM. The culture was grown for 18 h and then centrifuged at 4500 rpm for 10 min at 4°C. The cell pellet derived from 1 L of culture was resuspended in 35 mL of lysis buffer (50 mM HEPES sodium salt pH 8.0, 500 mM NaCl, 5% glycerol, 20 mM imidazole, 10 mM β-mercaptoethanol) and stored at -80°C. The samples were thawed and the cells were disrupted by sonication using bursts totaling 5 min in duration, with appropriate intervals for cooling. The cell debris was then pelleted by centrifugation at 15,000 rpm for 30 min at 4°C. The supernatant was applied to a

column packed with 10 mL of HisTrap HP resin (GE Healthcare), connected to a VacMan (Promega) and the chromatographic process was accelerated with a vacuum pump. The column was washed with 20 bed volumes of lysis buffer, and the His_6-tagged P5CRs were eluted with 25 mL of elution buffer (50 mM HEPES pH 8.0, 500 mM NaCl; 500 mM imidazole; 2 mM DTT). The His_6-tag was cleaved with TEV protease (2 mg of a His_6-tagged form) overnight at 4°C, and dialysis to remove the excess imidazole was carried out simultaneously. The resulting solution was mixed with His-Trap HP resin to capture the cleaved His_6-tag and the His_6-tagged TEV protease with the flow through containing the DapE protein, which was collected and concentrated. The next step required running the sample through a HiLoad 16/600 Superdex 200 Prep Grade column and eluting with the crystallization buffer.

Crystal Structure of NmDapE at 1.3 Å Resolution

Crystals were grown using freshly purified protein (~20 mg/ml) by the sitting drop method at 17 °C employing a precipitant solution of 0.2 M Li_2SO_4, 0.1 M Tris (pH 8.5), 1.26 M $(NH_4)_2SO_4$ and 0.05 M DMSO over several weeks. The crystals belonged to the $P2_12_12_1$ space group with unit cell parameters of a = 74.8 Å, b = 88.6Å, c = 133.4 Å and $\alpha = \beta = \gamma = 90°$ with a single dimer in the asymmetric unit (Table S1), consistent with *Nm*DapE in solution, which is a dimer. Prior to data collection, the mother liquor containing 25% glycerol was used as a cryoprotectant. A single crystal was picked up with a MiTeGen loop and flash-frozen in liquid nitrogen. The data set was collected at the 19-ID[17] beamline of the Structural Biology Center at the Advanced Photon Source, Argonne National Laboratory. All data sets were processed using the HKL3000[18] suite of programs. Data collection statistics are presented in Table S1. The high-resolution crystal structure of DapE was determined using the molecular replacing method employing the program MolRep[19] using the previously determined structure of *Nm*DapE. Cycles

of manual corrections of the model were carried out in the program COOT,[20] and the refinement routine was implemented in the program Refmac.fva.[21] The crystals diffracted to near atomic resolution, 1.30 Å, compared to the best resolution previously obtained for a DapE structure of 1.80 Å. This improvement in resolution allowed us to refine the structure anisotropically and to determine more detailed and accurate positions of atoms, reliable recognition of alternative conformations, and the correct positions of hydrogen atoms. This in turn enables more accurate docking and molecular dynamics studies that will ultimately enhance inhibitor design. The model of the structure has R_{work}/R_{free} = 11/15%. Analysis and validation of the structure was performed with the aid of MOLPROBITY and COOT validation tools.[22, 23] Figures were prepared using VMD.[24] The atomic coordinates and the structure factor file for this new open form of *Nm*DapE have been deposited in the RCSB Protein Bank with accession code 5UEJ.

Enzyme assays

DapE Enzyme Inhibition by Sulfate: IC_{50} *determination*

The inhibition of *Hi*DapE by sulfate was assessed using lithium sulfate following the protocol detailed by us previously[6] with slight modifications as detailed below. All inhibition assays were conducted with a reaction volume of 200 μL, 2 mM N^6-methyl-L,L-SDAP and 8 nM *Hi*DapE. To a 50 mM HEPES, pH 7.5 buffered solution at 0 °C was added lithium sulfate followed by *Hi*DapE and incubated for 10 min. N^6-Methyl-L,L-SDAP was added and allowed to react for 10 min followed by heating to 100 °C for 1 min and cooled on ice to 0 °C. A 2% ninhydrin solution (100 μL) was added, and the mixture was vortexed. The reaction was heated to 80 °C for 15 min followed by cooling on ice. The absorbance of an 80 μL aliquot was recorded at 570 nm on a BioTek Synergy 2 microplate reader. The inhibition assay of *Hi*DapE by lithium sulfate was performed in triplicate, and the IC_{50} was determined to be 13.8 ± 2.8 mM.

The IC_{50} and kinetics constants were obtained by fitting the data following modified Hill equation: $V = V_0 + (V_{max} - V_0) X^{nH} / (X^{nH}_{0.5} + X^{nH})$ using the graphing suite Origin 9.1 with the Levenberg-Marquardt non-linear least-squares algorithm.[25, 26] The velocity in the absence of the substrate is V_0, the velocity at saturating concentrations of the substrate or with no inhibitor for the inhibition assay is V_{max}, X is the concentration of the substrate or inhibitor, $X_{0.5}$ is the substrate ($S_{0.5}$) and inhibitor ($I_{0.5}$) concentration at 50% maximum velocity and at 50% inhibition, respectively. The Hill coefficient is represented as n_H. The inhibition plot is included in the Supplemental as Figures S3.

Kinetic studies

A discontinuous kinetic assay was performed on a Techne PCR Thermal Cycler System utilizing a modified ninhydrin assay protocol[6]. The volume of each component was adjusted to fit the total reaction volume of 50 µL and the enzyme concentration was 0.12 µM. Inhibition of *Hi*DapE with 10 mM, 20 mM, and 30 mM lithium sulfate was studied in triplicate while changing the substrate concentration from 0.5 mM to 5.5 mM. The amount of *N*-methyl-L,L-DAP formed over 10 minutes was monitored by measuring the absorbance of the complex formed by reacting *N*-methyl-L,L-DAP with 2% ninhydrin. The enzymatic activity was reported as the rate of formation of the product, *N*-methyl-L,L-DAP in absorbance unit per minute (AU/min). The kinetic constants were reproducible within ± 11% using the modified Hill equation utilizing the Levenberg-Marquardt non-linear least-squares algorithm.[25]

Sequence Comparisons

The non-repetitive sequence database was searched for homologs of *Nm*DapE using the blastp algorithm.[27] The sequences for the 99 DapE proteins found were aligned using the Clustal Omega algorithm [28]

Targeted Molecular Dynamics

The starting structure for Targeted Molecular Dynamics experiments was the new PDB 5UEJ structure. The target structure used for these simulations was a homology model of the closed structure (PDB 5VO3) that had the sequence of the open structure (PDB 5UEJ), and was created using SwissModel.[29] The two sequences were 55.1% identical, which is sufficient to produce a good homology model.[30] The structural assessment of the model using the tools available through Swiss-Model showed that it was a high-quality model. For molecular dynamics experiments, each simulation box containing either the open or the closed conformation of DapE, the substrate, and the catalytic zinc ions was assembled using the molecular graphics program VMD.[24] The simulation box was then brought to equilibrium using the molecular dynamics program NAMD.[31] The equilibration procedure involved energy minimization with and without restraints on the protein coordinates (6 ps each), slow heating from 10 to 310 K (60 ps), and then pressure and temperature equilibration using a Langevin piston (20 ps). Finally, unrestrained dynamics for 2 ns was done before data were acquired. Periodic boundary conditions were used. The cutoffs for nonbonding (van der Waals and electrostatic) interactions were 15 Å. The switch distance was 13 Å, and a 1.0 1–4 scaling factor was used. In the TMD simulations, the force constant set for the calculations was 1000 kcal/mol/Å^2. The simulation was run for a total of 50 ns. All calculations were performed using CHARMM 36 parameters.[32-35] The zinc ion in this forcefield is represented by electrostatic and van der Waals potentials. The total interaction energy values were determined for every 0.1 ns in

each set of simulations. All molecular graphics diagrams were generated using VMD.[24] The sulfur atom coordinates from the sulfates in the crystal structure were used to assign the coordinates of the carboxylate carbon atoms found at both ends of the substrate. The rest of the substrate atoms were then built and the energy of the overall structure was minimized. In the closed structure, the product positions were used as a reference for where the substrate should be built. Once the substrate was constructed, a water box with 0.15 M NaCl was built enclosing both DapE and the substrate to neutralize charges and mimic a physiological environment for the enzyme and substrate. The structure was then equilibrated for 2 ns in order to allow each system to achieve a local minimum energy conformation. TMD simulations were then run for 50 ns using this equilibrated structure. The equilibrated structure was then re-equilibrated twice for an additional 2 ns each. The TMD simulations were then rerun twice for 50 ns using these re-equilibrated structures. The target structure used for these simulations was a homology model of the closed structure (PDB 5VO3) that had the sequence of the open structure (PDB 5UEJ), which was created using SwissModel.[29]

Results and Discussion

High-Resolution X-Ray Crystal Structure: Comparison and Flexibility of DapE Structures

As expected, the new high-resolution X-ray structure of *Nm*DapE (PDB 5UEJ) shares many of the aspects of previously reported *Hi*DapE structures. *Hi*DapE and *Nm*DapE share a very high sequence homology of 55 % with no sequence gaps and bear the same active site architectures including metal binding residues and substrate binding residues necessary for hydrolytic activity.[14] Both are dimers with two domains in each chain (Figure 2A). The catalytic domain is globular and contains two Zn^{2+} ions and most of the catalytic residues. The

catalytic domain in the new *Nm*DapE open structure interacts with the communications domain of the other subunit, but the communications domains from the two chains form most of the inter-subunit contacts. There is a significant conformational change observed between the open and closed forms of the enzyme, which likely occurs upon substrate binding (Figures 2A and 2B).

Comparison of three different DapE crystal structures (5UEJ, 5VO3, and 3IC1) reveals significant differences in the orientations of the domains (Figure 2C-E). The dramatic change from the open to the closed conformation has been noted previously,[12, 36] but even the differences in conformations of available open structures (PDB 3IC1 and 5UEJ) are also striking, and comparison of eight different DapE structures (Figure S2) underscores the wide range of conformational flexibility of the DapE subunits. The products-bound structure manifests a different twist (Figure 2C) than the structures without product, and we have analyzed this change using conformationally sensitive dihedral angles (Figures S1 and S2). Conformational differences may also be due in part to differences in the crystallization conditions (Table S2), and there are many examples where different domain or subunit contacts are found for the same protein due to different crystallization conditions. For example, over 30 years ago Schiffer and co-workers[37] found that the domains of a Bence-Jones protein could adopt different domain associations depending on the crystallization conditions. For the Bence-Jones structures, the structural changes are limited to the way in which the domains are associated rather than to the folding of the domains themselves, and this is also true for the DapE structures. This ability to adopt different domain arrangements is due to the domains being connected by only one polypeptide strand in the case of Bence-Jones protein or two strands of a polypeptide chain in the case of DapE, allowing flexibility between domains.

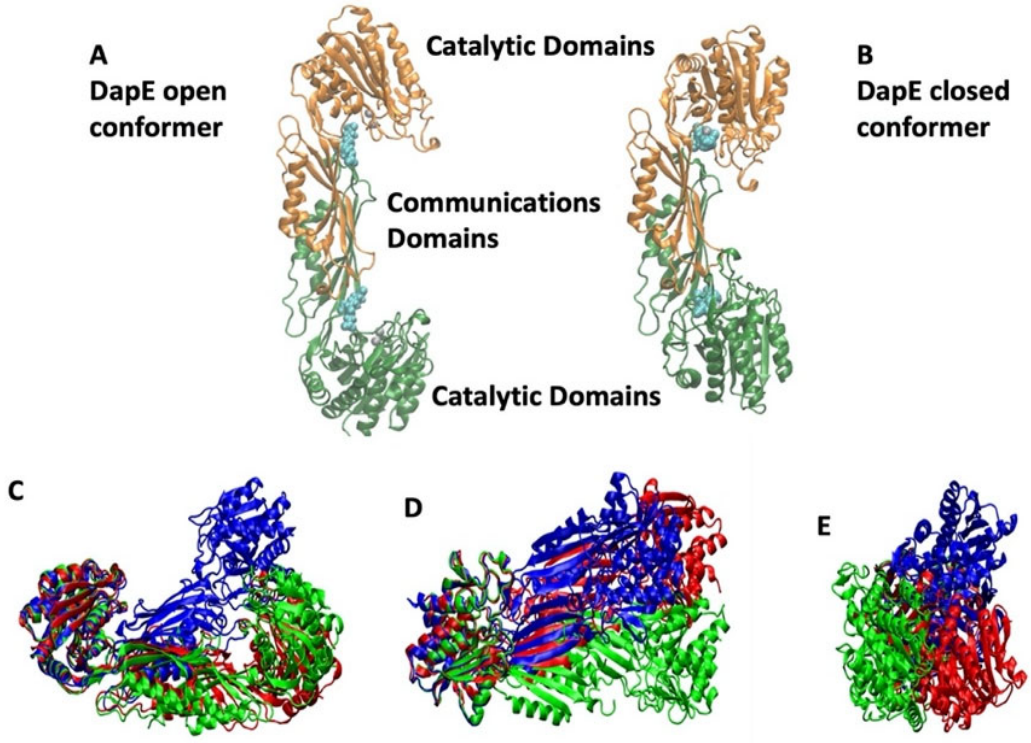

Figure 2: DapE enzyme X-ray crystal structures illustrating conformational changes. (A) DapE open conformation of *Nm*DapE (PDB 5UEJ) with the substrate shown in blue space-filling atoms modeled in the active site; (B) closed conformation of *Hi*DapE (PDB 5VO3) with the bound substrate modeled in space-filling blue atoms; Panels (C), (D), and (E) show overlap of three different DapE structures: the new high-resolution open *Nm*DapE structure PDB 5UEJ in red, the 2.30 Å resolution open *Hi*DapE structure PDB 3IC1 in green, and the products-bound *Nm*DapE structure PDB 5VO3 in blue. The A-chains for all three proteins are superimposed on the left side of Figures 2C-E showing the different positions of the B chains on the right side of each representation, with each panel showing mutually perpendicular views of the three overlapped structures.

Hinge-like motions caused by different crystal environments have been seen in many other proteins,[38, 39] along with the ability of crystal packing contacts to cause these variations.[40, 41] On the other hand, there are even more examples of different domain or subunit arrangements that occur due to the binding of a ligand.[42] The conformational change due to binding of the products by DapE (PDB 5VO3 in Fig. 2B) is different than the range of flexibility seen for the DapE structures without bound products. A significant twist in the conformation of DapE is

demonstrated by changes in selected dihedral angles (Figures S1 and S2) that are notably different for the products-bound structure.

Inhibition of DapE by Sulfate

We observed that two sulfate ions are bound in the new open *Nm*DapE structure (5UEJ) and hypothesized that these sulfates from the crystallization buffer occupy the same locations occupied by two of the negatively-charged carboxylates of the substrate. This was confirmed by direct comparison of the products-bound *Hi*DapE closed structure (5VO3) with the sulfate-bound *Nm*DapE open structure (5UEJ), where the carboxylates are observed to electrostatically bind to Arg178 and Arg258 of *Hi*DapE, analogous to the sulfates binding Arg179 and Arg259 of *Nm*DapE, respectively (Figure 3). Arginine residues were found in these positions in all of the 99 sequences similar to *Nm*DapE found by a blastp search. Reviewing all eleven DapE structures deposited in the PDB (summarized in Table S2), six of the crystal structures are observed to have one or two sulfates bound in their active sites. DapE crystal structures with at least one bound sulfate in the active sites include PDBs 3IC1 and 3ISZ,[10] as well as PDBs 4O23, 4PPZ, and 4PQA.[11] The DapE structure that was first reported is an apo structure, 1VGY[9] that lacks bound sulfates, although crystallization conditions were not reported, making it impossible to know if sulfate ions were present in the crystallization solution. Several truncated DapE proteins have been expressed lacking the linker domains and were crystallized in the presence of acetate rather than sulfate (PDBs 4ONW, 4OP4, and 4H2K),[43] and therefore do not have bound sulfate, but neither do they exhibit bound acetate in their active sites. These truncated DapE proteins are either missing the Arg residues that bind the sulfates, or these Arg residues are near the new termini of the protein and thus are in very flexible regions of the structure. Therefore, sulfate binding to these residues would not be expected. Sulfates are well known to bind at

protein phosphate sites,[44, 45] and sulfate ions can also compete with carboxylate ions for binding sites.[46]

Realizing that sulfate may compete with the substrate in the active site, we determined the inhibitory potency of sulfate to be IC_{50} = 13.8 ± 2.8 mM using our ninhydrin-based assay (Figure S3).[6] The concentration of sulfate in the crystallization buffer of PDB 5UEJ was 1.46 M, which is 106X higher than the IC_{50} of sulfate, consistent with its presence in the active site. The only reported products-bound structure (5VO3) did not have sulfate in its crystallization buffer, which was likely more advantageous for substrate binding given the absence of competing sulfate. In order to investigate the nature of sulfate binding to the DapE active site we performed a kinetic assay varying the substrate and sulfate concentrations. The sulfate inhibition of *Hi*DapE followed a competitive inhibition pattern as summarized in Table 1 and the saturation curves are reported in Supplemental as Figure S4, S5, S6, S7 and S8. The saturation of activity with increasing substrate concentration was not observed, rather the enzymatic activity was inconsistent as the pH of the solution started to decline with increasing *N*-methyl-L,L-SDAP substrate concentration above 5.5 mM. The decrease in the pH of the solution was attributed the to the fact that *N*-methyl-L,L-SDAP was synthesized and used as the trifluoroacetate salt of the amine, hence at higher concentrations it ultimately affects the pH of the solution.

Table 1: Kinetic parameters for *Hi*DapE with *N*-methyl-L,L-SDAP substrate.

Assay	Sulfate (mM)	V_{max} (AU/min)	$S_{0.5}$ (mM)
Control	0	0.068 ± 0.0055	1.21 ± 0.15
Inhibition	10	0.073 ± 0.0072	2.50 ± 0.29
	20	0.080 ± 0.0098	2.72 ± 0.066

	30	0.084 ± 0.0052	2.92 ± 0.098

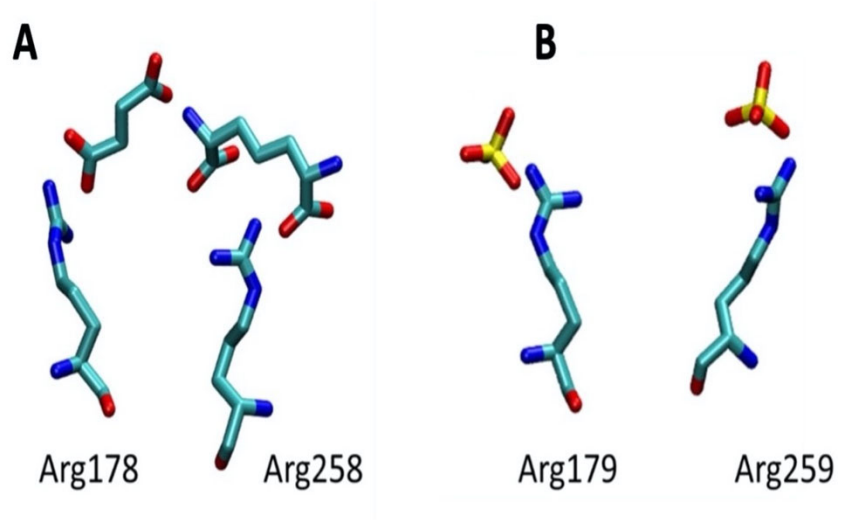

Figure 3. Key Coulombic interactions of (A) the terminal substrate-derived carboxylates of the products in *Hi*DapE (PDB 5VO3) with Arg178 and Arg259, and (B) the two bound sulfate ions in the open conformation of *Nm*DapE (PDB 5UEJ) with the corresponding arginine residues Arg179 and Arg259, respectively.

Targeted Molecular Dynamics

The open conformation DapE structures, including the new high-resolution structure, in comparison with our products-bound closed X-ray crystal structure[12] reveal the dynamic conformational change between the open and closed states of DapE (Fig. 4). This conformational change was proposed to be induced by substrate binding, which is consistent with a hinge domain mechanism that enables both domains to interact with the substrate. The *Hi*DapE products-bound structure further revealed several new protein-ligand interactions that had not been predicted by docking or by molecular dynamics[47] including the demonstration of distinct succinate and diaminopimelic acid binding pockets, and that both domains play a key role in substrate recognition and catalysis.

To better understand the catalytically important conformational change of DapE from the open to the closed conformer, TMD simulations were performed. TMD involves application of an additional force on selected atoms in the direction of the positions of their counterparts in the target structure.[48, 49] This force depends on the number of atoms selected, the selected force constant, and the RMSD between the coordinates at any given time during the simulation and the final coordinates. Three TMD runs were performed from the open to the closed conformation using PDB 5UEJ for the open starting DapE conformation and 5VO3 for the closed target conformation. The selected atoms were either all the α-carbons in both subunits or all the α-carbons in just one of the two subunits. Prior to running TMD simulations, the native substrate L,L-SDAP was built into the active sites of both the initial and target structures and the system was relaxed as described in the Experimental section. In the open structure, placement of the substrate was guided by the positions of the two sulfate ions found in the active site of the PDB file to model the positions of the substrate terminal carboxylates. Substrate was placed into the active site of the closed structure in a manner consistent with the binding of the products in 5VO3.

The first TMD scenario applied a force to both subunits of DapE in the open conformation. Both subunits approached the closed conformation as measured by their degree of overlap with the target structure (Figures 4A and 4B). Furthermore, RMSD values comparing the initial structure to the target structure were calculated before and after the simulation to

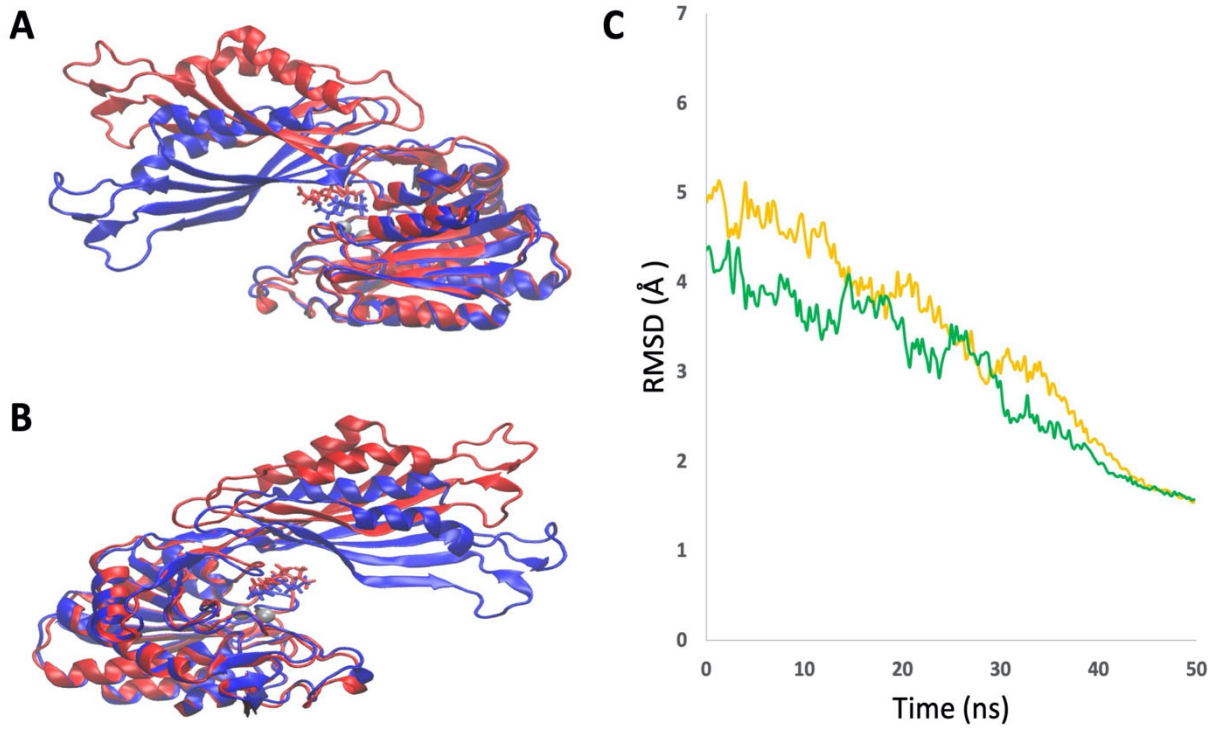

Figure 4. Images of subunit A (A) and subunit B (B) of the DapE enzyme overlaid at t = 0 (in red) and t = 50 ns (in blue) in the simulation with the force on both subunits. The substrate is also shown in both active sites in its position at t = 0 (in red) and t = 50 ns (in blue). Average RMSD between subunits A (in orange) and B (in green) in the open structure and their positions in the closed structure is shown in graph (C).

determine the degree of closure. The RMSD differences by subunit show near-complete convergence of the original open structure toward the target closed structure during each run (Figure 4C). The second and third TMD experiments involved applying the additional force only to subunit A, and then only to subunit B, respectively. These calculations were performed to investigate if closing one subunit might compel the other subunit to also begin closing. In the simulation with the force applied only to subunit A, that subunit closes as it did with the force applied to both subunits (Figure 5A), however subunit B does not close or converge toward the target coordinates to any significant extent (Figure 5B). The independence of the two subunits is also supported by the change in RMSD values between the initial structure and the target structure at the beginning and end of the simulation (Figure 5C). In the simulation with the force

applied only to subunit B, the simulation plays out in the reverse manner. Subunit B closes completely under these conditions whereas subunit A does not converge toward the target structure. Changes in the RMSD values between the initial and final structures support this observation that movement was only observed in the subunit to which force was applied (Figure S6A3).

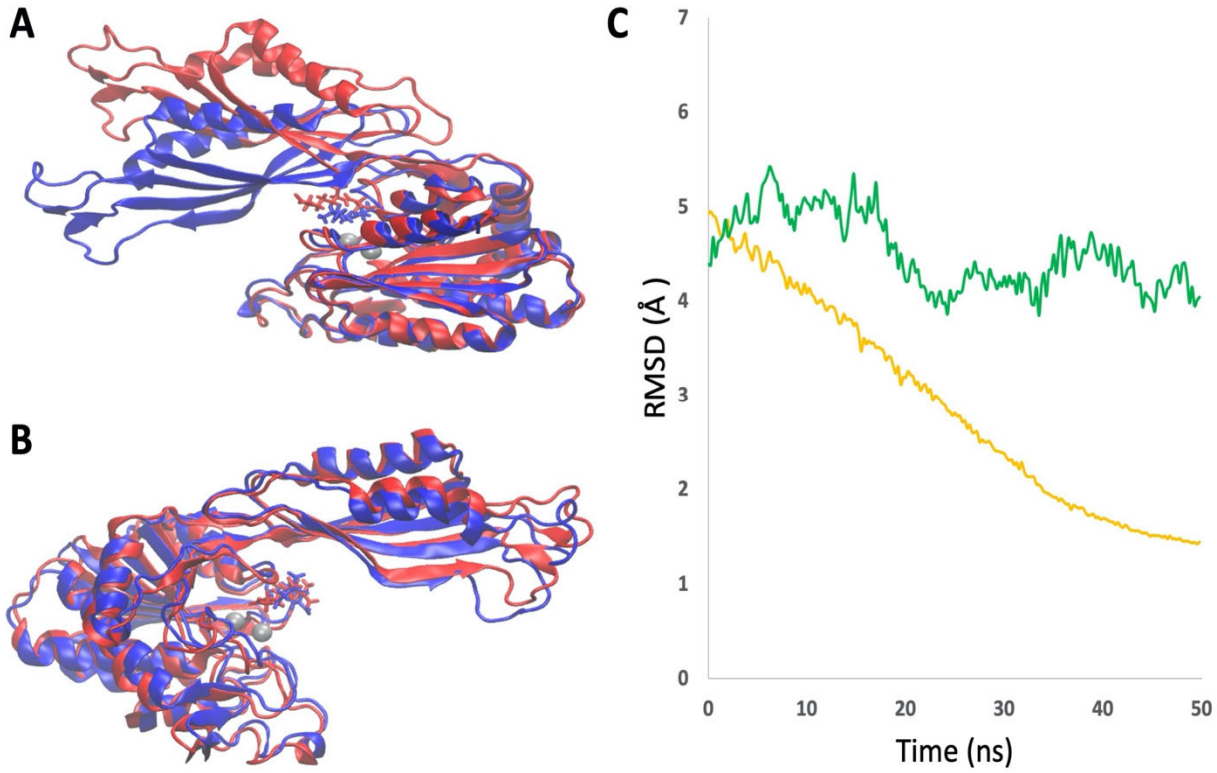

Figure 5. (A) Images of subunit A (A) and subunit B (B) of the DapE enzyme overlaid at t = 0 (in red) and t = 50 ns (in blue) in the simulation with the force only on subunit A. The substrate is also shown in both active sites in its position at t = 0 (in red) and t = 50 ns (in blue). Average RMSD between subunits A (in orange) and B (in green) in the open structure and their positions in the closed structure is shown in graph (C).

Although no force was applied to the substrate, L,L-SDAP, it moved due to its interactions with the protein. As the subunits in the open conformation close, the substrate becomes further enveloped within the active site, and the distance between it and the catalytic

zinc atoms decreases dramatically in both subunits in all three sets of simulations (Figure S6B1-3). The movement of the substrate is likely a result of the Coulombic attractions between two of the carboxyl groups in L,L-SDAP and Arg179 and Arg259, respectively, as well as a function of the movement of His195 from the communications domain of the opposite subunit. When observing the initial and final positions of the substrate in all three sets of simulations, the substrate interacts consistently with both arginine residues, while at t = 50 ns, His195 has moved into the active site in the closed conformation, enabling its critical interaction with the substrate.

The Arg179 and Arg259 residues interact with the substrate initially (Figure 3B) and throughout the simulation (Figures S6D1-3, S6E1-3, and S6G1-3), indicating that these arginine residues likely play a significant role in ferrying the substrate from its initial binding site further into the enzyme as it closes (Figures 6A and 6B). We had previously demonstrated inhibition of HiDapE by addition of the arginine-specific chemical modification reagent 2,3-butanedione, indicating that at least one arginine residue interacts with the substrate.[12] His195B, by contrast, is much further from the substrate but moves a significant distance (~6 Å) from the communications domain of the opposite subunit in order to participate in the active site and form the oxyanion hole that enables cleavage of the substrate.[12] His195B moves closer to the catalytic zinc atoms over the course of the conformational change and is in position to interact with the active site by the end of the simulation (Figures 7A-C and S6C1-3). This motion should contribute to an overall stabilization as the substrate moves further into the active site in the subunits that are closing. Calculated interaction energies between the substrate and the enzyme demonstrate that this is the case (Fig. 6C). The substrate binds more tightly as the protein closes.

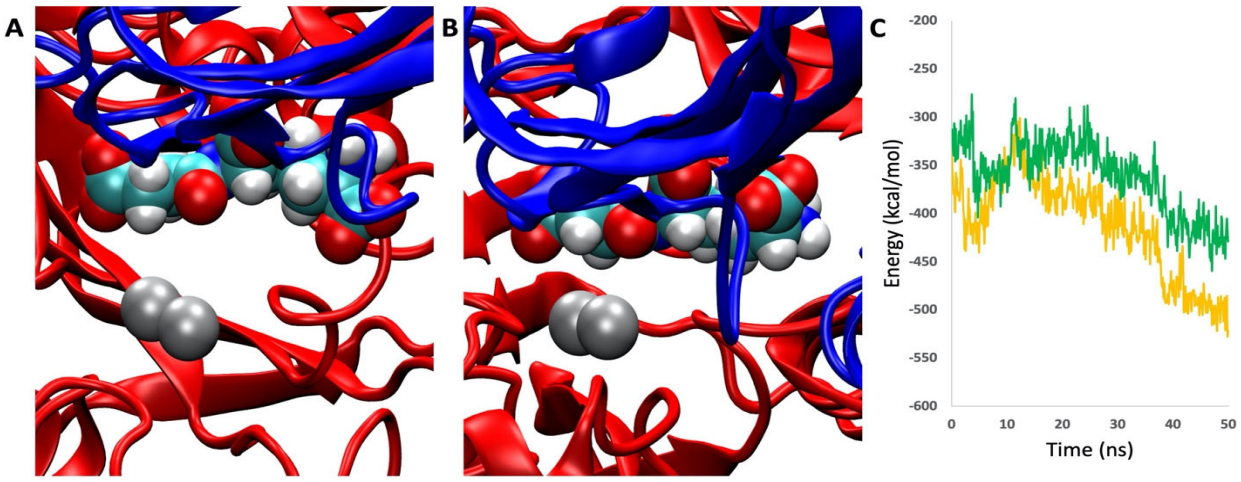

Figure 6. (A) Images of the active site of DapE at t = 0 (A) and t = 50 ns (B) with the substrate and the catalytic zinc atoms shown in the simulation with the force on both subunits. The interaction energy between the substrate and the enzyme in subunit A (in orange) and in subunit B (in green) is shown in graph (C).

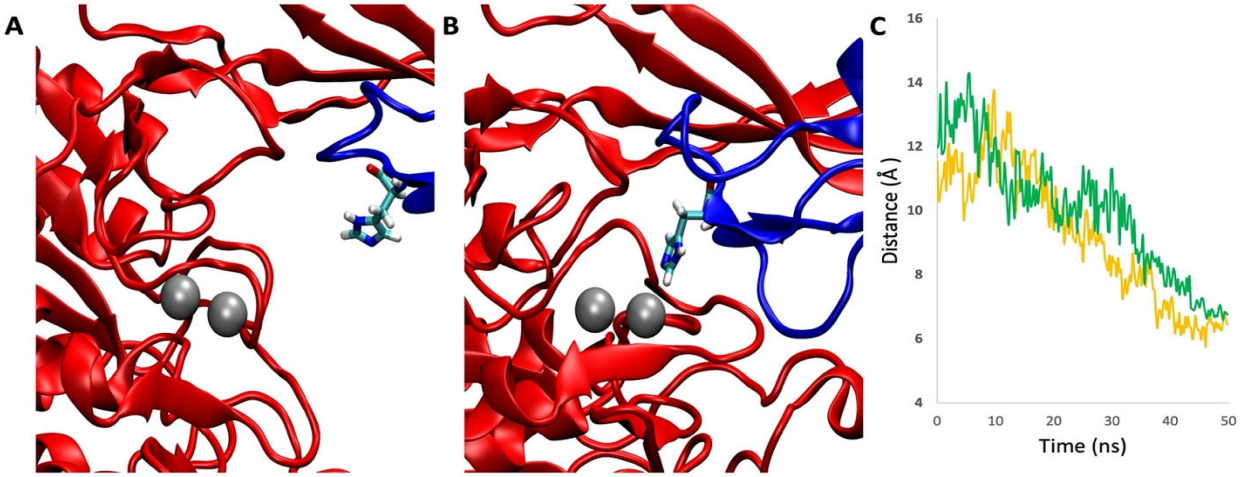

Figure 7. (A) Images of the active site of DapE at t = 0 (A) and t = 50 ns (B) with His195 and the catalytic zinc atoms shown in the simulation with the force on both subunits. The distance from His195 to those zinc atoms in subunit A (in orange) and in subunit B (in green) is shown in graph (C).

Conclusion

In summary, we have succeeded in crystallizing *Nm*DapE (PDB 5UEJ), an open conformation structure with atomic-level resolution (1.3 Å). Comparison with other DapE structures demonstrates the flexibility of this protein. The new structure reveals two sulfates hydrogen bound to active site Arg residues that have been implicated in substrate recognition and binding.[12] The presence of sulfate prompted us to determine the inhibitory potency of sulfate, which has an IC_{50} = 13.8 ± 2.8 mM. The sulfate positions suggested the binding site for the substrate in the open structure, and we then employed this new structure as the starting point for our targeted molecular dynamics simulations studying the dramatic conformational change from the open to the closed conformation that occurs when DapE binds its substrate L,L-SDAP. Addressing the possibility that the closure of the two subunits may be linked, these TMD studies reveal the independence of the two subunits. The TMD method enabled us to examine how different parts of the system might affect each other. By putting a force on only one of the subunits, we found that closing that subunit did not force the closure of the other subunit. Since the SDAP also did not have a force on it, the results showed how the substrate is pulled into position in the active site. Given our long-range goal of developing new antibiotics based on inhibitors of DapE, this was an important result. The conformational change of the protein results in the substrate moving towards the active site and increasing the binding affinity. These data provide new insight to the proposed catalytic mechanism as they confirm the ability of DapE to shift between an open conformation to a closed form upon the addition of substrate. They further confirm that His195B can move more than 6 Å into the A subunit active site, a critical step in the catalytic process. Furthmore, the design of DapE inhibitors as potential antibiotics with a new mechanism of action is critically important. An enhanced understanding of the key binding interactions in the active site will enable the de novo design of inhibitors as well as

optimization of existing lead structures. The sulfates bound in the active site in the new high-resolution DapE crystal structure underscore the importance of the Coulombic interactions in binding the negatively charged carboxylates in the substrate. Understanding the energetics and geometry changes at play in the closing of the DapE subunit revealed by TMD inform the design of potential inhibitors that can lead to a closed or partially-closed structure versus binding only to the open conformer of DapE.

ASSOCIATED CONTENT

Supporting Information. X-Ray Collection and refinement statistics, analysis of DapE conformational changes, plots of inhibition by sulfate, and graphical analyses of targeted molecular dynamics.

Protein Data Bank: PDB 5UEJ

AUTHOR INFORMATION

Corresponding Authors

E-mail: dbecke3@luc.edu

Accession Codes

Uniprot: DapE; Q9JYL2

Protein Data Bank: PDB 5UEJ

ORCID

Richard C. Holz 0000-0001-6093-2799

Daniel P. Becker: 0000-0001-9392-0460

Funding

This work was supported in part by the National Science Foundation (CHE-2003861, RCH)

Notes

The authors declare no competing financial interest.

References

1. World Health Organization Antibacterial agents in clinical development: an analysis of the antibacterial clinical development pipeline, including tuberculosis. **2017**, .

2. Klevens, R. M.; Morrison, M. A.; Nadle, J.; Petit, S.; Gershrnan, K.; Ray, S.; Harrison, L. H.; Lynfield, R.; Dumyati, G.; Townes, J. M.; Craig, A. S.; Zell, E. R.; Fosheim, G. E.; Mcdougal, L. K.; Carey, R. B.; Fridkin, S. K. Invasive methicillin-resistant staphylococcus aureus infections in the United States. *JAMA, J. Am. Med. Assoc.* **2007**, *298,* 1763-1771.

3. Howe, R. A.; Bowker, K. E.; Walsh, T. R.; Feest, T. G.; MacGowan, A. P. Vancomycin-resistant Staphylococcus aureus. *Lancet* **1998**, *351,* 602.

4. Gillner, D. M.; Becker, D. P.; Holz, R. C. Lysine biosynthesis in bacteria: a metallodesuccinylase as a potential antimicrobial target. *JBIC, J. Biol. Inorg. Chem.* **2013**, *18,* 155-163.

5. Scapin, G.; Blanchard, J. S. Enzymology of bacterial lysine biosynthesis. *Adv. Enzymol. Relat. Areas Mol. Biol.* **1998**, *72,* 279-324.

6. Heath, T. K.; Lutz Jr, M. R.; Reidl, C. T.; Guzman, E. R.; Herbert, C. A.; Nocek, B. P.; Holz, R. C.; Olsen, K. W.; Ballicora, M. A.; Becker, D. P. Practical spectrophotometric assay for the dapE-encoded N-succinyl-L, L-diaminopimelic acid desuccinylase, a potential antibiotic target. *PloS one* **2018**, *13,* e0196010.

7. Karita, M.; Etterbeek, M. L.; Forsyth, M. H.; Tummuru, M. K. R.; Blaser, M. J. Characterization of Helicobacter pylori dapE and construction of a conditionally lethal dapE mutant. *Infect. Immun.* **1997**, *65,* 4158-4164.

8. Pavelka, M. S., Jr.; Jacobs, W. R.,Jr Biosynthesis of diaminopimelate, the precursor of lysine and a component of peptidoglycan, is an essential function of Mycobacterium smegmatis. *J. Bacteriol.* **1996**, *178,* 6496-6507.

9. Badger, J.; Sauder, J.; Adams, J.; Antonysamy, S.; Bain, K.; Bergseid, M.; Buchanan, S.; Buchanan, M.; Batiyenko, Y.; Christopher, J. Structural analysis of a set of proteins resulting from a bacterial genomics project. *Proteins: Structure, Function, and Bioinformatics* **2005**, *60,* 787-796.

10. Nocek, B. P.; Gillner, D. M.; Fan, Y.; Holz, R. C.; Joachimiak, A. Structural Basis for Catalysis by the Mono- and Dimetalated Forms of the dapE-Encoded N-succinyl-L,L-Diaminopimelic Acid Desuccinylase. *J. Mol. Biol.* **2010**, *397,* 617-626.

11. Starus, A.; Nocek, B.; Bennett, B.; Larrabee, J. A.; Shaw, D. L.; Sae-Lee, W.; Russo, M. T.; Gillner, D. M.; Makowska-Grzyska, M.; Joachimiak, A.; Holz, R. C. Inhibition of the dapE-Encoded N-Succinyl-L,L-diaminopimelic Acid Desuccinylase from Neisseria meningitidis by L-Captopril. *Biochemistry* **2015**, *54,* 4834-4844.

12. Nocek, B.; Reidl, C.; Starus, A.; Heath, T.; Bienvenue, D.; Osipiuk, J.; Jedrzejczak, R. P.; Joachimiak, A.; Becker, D. P.; Holz, R. C. Structural Evidence for a Major Conformational Change Triggered by Substrate Binding in DapE Enzymes: Impact on the Catalytic Mechanism. *Biochemistry (N. Y.)* **2018**, *57,* 574.

13. Reidl, C.; Majorek, K. A.; Dang, J.; Tran, D.; Jew, K.; Law, M.; Payne, Y.; Minor, W.; Becker, D. P.; Kuhn, M. L. Generating enzyme and radical-mediated bisubstrates as tools for investigating Gcn5-related N-acetyltransferases. *FEBS Lett.* **2017**, *591,* 2348-2361.

14. Reidl, C. T.; Heath, T. K.; Darwish, I.; Torrez, R. M.; Moore, M.; Gild, E.; Nocek, B. P.; Starus, A.; Holz, R. C.; Becker, D. P. Indoline-6-Sulfonamide Inhibitors of the Bacterial Enzyme DapE. *Antibiotics* **2020**, *9,* 595.

15. Dutta, D.; Mishra, S. L-Captopril and its derivatives as potential inhibitors of microbial enzyme DapE: A combined approach of drug repurposing and similarity screening. *J. Mol. Graph. Model.* **2018**, *84,* 82-89.

16. Mandal, R. S.; Das, S. In silico approach towards identification of potential inhibitors of Helicobacter pylori DapE. *J. Biomol. Struct. Dyn.* **2015**, *33,* 1460-1473.

17. Rosenbaum, G.; Alkire, R. W.; Evans, G.; Rotella, F. J.; Lazarski, K.; Zhang, R.; Ginell, S. L.; Duke, N.; Naday, I.; Lazarz, J. The Structural Biology Center 19ID undulator beamline: facility specifications and protein crystallographic results. *Journal of synchrotron radiation* **2006**, *13,* 30-45.

18. Minor, W.; Cymborowski, M.; Otwinowski, Z.; Chruszcz, M. HKL-3000: the integration of data reduction and structure solutionâ€“from diffraction images to an initial model in minutes. *Acta Crystallogr. , Sect. D: Biol. Crystallogr.* **2006**, *62,* 859.

19. Vagin, A.; Teplyakov, A. MOLREP: an automated program for molecular replacement. *Journal of applied crystallography* **1997**, *30,* 1022-1025.

20. Emsley, P.; Lohkamp, B.; Scott, W. G.; Cowtan, K. Features and development of Coot. *Acta Crystallographica Section D: Biological Crystallography* **2010**, *66,* 486-501.

21. Murshudov, G. N.; SkubÃ¡k, P.; Lebedev, A. A.; Pannu, N. S.; Steiner, R. A.; Nicholls, R. A.; Winn, M. D.; Long, F.; Vagin, A. A. REFMAC5 for the refinement of macromolecular crystal structures. *Acta Crystallogr. , Sect. D: Biol. Crystallogr.* **2011**, *67,* 355.

22. Davis, I. W.; Leaver-Fay, A.; Chen, V. B.; Block, J. N.; Kapral, G. J.; Wang, X.; Murray, L. W.; Arendall, W. B.,3rd; Snoeyink, J.; Richardson, J. S.; Richardson, D. C. MolProbity: all-atom contacts and structure validation for proteins and nucleic acids. *Nucleic Acids Res* **2007**, *35,* W375-83.

23. Emsley, P.; Cowtan, K. Coot: model-building tools for molecular graphics. *Acta Crystallogr. , Sect. D: Biol. Crystallogr.* **2004**, *D60,* 2126-2132.

24. Humphrey, W.; Dalke, A.; Schulten, K. VMD: visual molecular dynamics. *J Mol Graph* **1996**, *14,* 33-8, 27-8.

25. Press, W. H.; Flannery, B. P.; Teukolsky, S. A.; Vetterling, W. T. ***Numerical Recipes in C: The Art of Scientific Computing****;* Cambridge University Press, New York: 1988; .

26. Figueroa, C. M.; Esper, M. C.; Bertolo, A.; Demonte, A. M.; Aleanzi, M.; Iglesias, A. A.; Ballicora, M. A. Understanding the allosteric trigger for the fructose-1,6-bisphosphate regulation of the ADP-glucose pyrophosphorylase from Escherichia coli. *Biochimie* **2011**, *93,* 1816-1823.

27. Altschul, S. F.; Gish, W.; Miller, W.; Myers, E. W.; Lipman, D. J. Basic local alignment search tool. *J. Mol. Biol.* **1990**, *215,* 403-410.

28. Sievers, F.; Wilm, A.; Dineen, D.; Gibson, T. J.; Karplus, K.; Li, W.; Lopez, R.; McWilliam, H.; Remmert, M.; Soding, J.; Thompson, J. D.; Higgins, D. G. Fast, scalable generation of high-quality protein multiple sequence alignments using Clustal Omega. *Mol. Syst. Biol.* **2011**, *7,* 539.

29. Waterhouse, A.; Bertoni, M.; Bienert, S.; Studer, G.; Tauriello, G.; Gumienny, R.; Heer, F. T.; de Beer, Tjaart A P; Rempfer, C.; Bordoli, L. SWISS-MODEL: homology modelling of protein structures and complexes. *Nucleic Acids Res.* **2018**, *46,* W296-W303.

30. Waterman, M. S.; Eggert, M. A new algorithm for best subsequence alignments with application to tRNA-rRNA comparisons. *J. Mol. Biol.* **1987**, *197,* 723-728.

31. Phillips, J. C.; Braun, R.; Wang, W.; Gumbart, J.; Tajkhorshid, E.; Villa, E.; Chipot, C.; Skeel, R. D.; Kale, L.; Schulten, K. Scalable molecular dynamics with NAMD. *J. Comput. Chem.* **2005**, *26,* 1781-1802.

32. Vanommeslaeghe, K.; Hatcher, E.; Acharya, C.; Kundu, S.; Zhong, S.; Shim, J.; Darian, E.; Guvench, O.; Lopes, P.; Vorobyov, I. CHARMM general force field: A force field for drugâ€ like molecules compatible with the CHARMM allâ€ atom additive biological force fields. *Journal of computational chemistry* **2010**, *31,* 671-690.

33. Best, R. B.; Zhu, X.; Shim, J.; Lopes, P. E.; Mittal, J.; Feig, M.; MacKerell Jr, A. D. Optimization of the additive CHARMM all-atom protein force field targeting improved sampling of the backbone ϕ, ψ and side-chain χ1 and χ2 dihedral angles. *Journal of chemical theory and computation* **2012**, *8,* 3257-3273.

34. MacKerell Jr, A. D.; Feig, M.; Brooks, C. L. Improved treatment of the protein backbone in empirical force fields. *J. Am. Chem. Soc.* **2004**, *126,* 698-699.

35. MacKerell Jr, A. D.; Bashford, D.; Bellott, M.; Dunbrack Jr, R. L.; Evanseck, J. D.; Field, M. J.; Fischer, S.; Gao, J.; Guo, H.; Ha, S. All-atom empirical potential for molecular modeling and dynamics studies of proteins. *The journal of physical chemistry B* **1998**, *102,* 3586-3616.

36. DÃaz-SÃ¡nchez, Ã G.; Terrazas-LÃ³pez, M.; Aguirre-Reyes, L. G.; Lobo-Galo, N.; Ã lvarez-Parrilla, E.; MartÃnez-MartÃnez, A. Aspectos estructurales y funcionales de la N-Succinil-L, L-diaminopimelato desuccinilasa, una enzima clave para el crecimiento bacteriano y un blanco para el control antimicrobiano. *TIP.Revista especializada en ciencias quÃmico-biolÃ³gicas* **2019**, *22,* .

37. Schiffer, M.; Ainsworth, C.; Xu, Z.; Carperos, W.; Olsen, K.; Solomon, A.; Stevens, F.; Chang, C. Structure of a second crystal form of Bence-Jones protein Loc: strikingly different

domain associations in two crystal forms of a single protein. *Biochemistry (N. Y.)* **1989**, *28,* 4066-4072.

38. Eyal, E.; Gerzon, S.; Potapov, V.; Edelman, M.; Sobolev, V. The limit of accuracy of protein modeling: influence of crystal packing on protein structure. *J. Mol. Biol.* **2005**, *351,* 431-442.

39. Joshi, M.; Gakhar, L.; Fuentes, E. J. High-resolution structure of the Tiam1 PHn-CC-Ex domain. *Acta Crystallographica Section F: Structural Biology and Crystallization Communications* **2013**, *69,* 744-752.

40. Thompson, H. P.; Day, G. M. Which conformations make stable crystal structures? Mapping crystalline molecular geometries to the conformational energy landscape. *Chemical Science* **2014**, *5,* 3173-3182.

41. Luo, J.; Liu, Z.; Guo, Y.; Li, M. A structural dissection of large protein-protein crystal packing contacts. *Scientific reports* **2015**, *5,* 14214.

42. Ahmad, E.; Rabbani, G.; Zaidi, N.; Khan, M. A.; Qadeer, A.; Ishtikhar, M.; Singh, S.; Khan, R. H. Revisiting ligand-induced conformational changes in proteins: essence, advancements, implications and future challenges. *Journal of Biomolecular Structure and Dynamics* **2013**, *31,* 630-648.

43. Nocek, B.; Starus, A.; Makowska-Grzyska, M.; Gutierrez, B.; Sanchez, S.; Jedrzejczak, R.; Mack, J. C.; Olsen, K. W.; Joachimiak, A.; Holz, R. C. The dimerization domain in DapE enzymes is required for catalysis. *PLoS One* **2014**, *9,* e93593/1-e93593/11, 11.

44. Kanyo, Z. F.; Christianson, D. W. Biological recognition of phosphate and sulfate. *J. Biol. Chem.* **1991**, *266,* 4264-4268.

45. Copley, R. R.; Barton, G. J. **A Structural Analysis of Phosphate and Sulphate Binding Sites in Proteins: Estimation of Propensities for Binding and Conservation of Phosphate Binding Sites**. *Journal of Molecular Biology* **1994**, *242,* 321-329.

46. Moras, D.; Olsen, K. W.; Sabesan, M. N.; Buehner, M.; Ford, G. C.; Rossmann, M. G. Studies of asymmetry in the three-dimensional structure of lobster D-glyceraldehyde-3-phosphate dehydrogenase. *J. Biol. Chem.* **1975**, *250,* 9137-9162.

47. Dutta, D.; Mishra, S. Structural and mechanistic insight into substrate binding from the conformational dynamics in apo and substrate-bound DapE enzyme. *Phys Chem Chem Phys* **2016**, *18,* 1671-1680.

48. Weng, J.; Fan, K.; Wang, W. The conformational transition pathways of ATP-binding cassette transporter BtuCD revealed by targeted molecular dynamics simulation. *PLoS One* **2012**, *7,* e30465.

49. Cheng, X.; Wang, H.; Grant, B.; Sine, S. M.; McCammon, J. A. Targeted molecular dynamics study of C-loop closure and channel gating in nicotinic receptors. *PLoS Comput. Biol.* **2006**, *2,* e134.